ARTICLE NO. 78-284

Numerical Solution for Airfoils near Stall in Optimized Boundary-Fitted Curvilinear Coordinates

James K. Hodge*
Air Force Flight Test Center, Edwards Air Force Base, Calif.
Alan L. Stone*
Air Force Acquisitions Logistics Division, Wright-Patterson Air Force Base, Ohio
and
Thomas E. Miller*
Air Force Flight Dynamics Laboratory, Wright-Patterson Air Force Base, Ohio

Boundary-fitted curvilinear coordinate systems are optimized for viscous flows about arbitrary airfoils at angles of attack such that boundary-layer-dependent grid systems for high Reynolds numbers are generated efficiently. The grid systems are utilized in implicit finite-difference solutions. Solution of a one-dimensional model equation is compared with the theoretical solution. The unsteady Navier-Stokes equations are solved for the incompressible flow around a cylinder and around NACA airfoils approaching stall. The predicted flows around a NACA 6412 airfoil near stall at Reynolds numbers of 4×10^4 and 2×10^5 are compared with the experimental observations obtained in a smoke tunnel.

Nomenclature

A_K = amplitude coefficients for contracting mesh systems
C_D = drag coefficient
C_L = lift coefficient
C_P = pressure coefficient
C_1, C_2, C_3, C_4 = contours in a doubly connected region
D = velocity divergence
D_1, D_2 = coordinate-transformation parameter, Eq. (11)
D_K = decay coefficients for contracting mesh systems
IMAX = number of ξ lines in transformed plane
J = Jacobian determinant
JMAX = number of η lines in transformed plane
K = number of points in boundary layer
L = characteristic length
p = nondimensional pressure ($C_p/2$)
P, Q = summations of exponential functions for contraction of mesh systems
R = two-dimensional physical region
Re = Reynolds number
S = Strouhal number based on thickness
t = time
T = nondimensional time (Ut/L)
u = nondimensional velocity component in x direction
U = freestream velocity magnitude
v = nondimensional velocity component in y direction
x, y = nondimensional physical field coordinates
α = coordinate-transformation parameter, Eq. (2)
β = coordinate-transformation parameter, Eq. (2)
γ = coordinate-transformation parameter, Eq. (2)
η = transformed coordiante
ξ = tranformed coordinate
σ = coordinate-transformation parameter, Eq. (11)
τ = coordinate-transformation parameter, Eq. (11)
ϕ = angle of attack
Φ = acceleration parameter
μ = function definition, Eq. (6)

Superscripts

N = time step index
(s) = iterate number
$*$ = the transformed plane

Subscripts

i, j = field position in mesh systems
CS = central-space difference
x, y, η, ξ, T = first partial differentiation
$xx, yy, \eta\eta, \xi\xi$ = second partial differentiation
$\xi\eta$ = cross partial differentiation
∞ = value at infinity

Presented as Paper 78-284 at the AIAA 16th Aerospace Sciences Meeting, Huntsville, Ala., Jan. 16-18, 1978; submitted March 9, 1978; revision received Oct. 16, 1978.

Index categories: Computational Methods; Boundary Layers and Convective Heat Transfer—Laminar; Jets, Wakes, and Viscid-Inviscid Flow Interactions.

*Captain, U.S. Air Force. Member AIAA.

Introduction

THE calculation of the operating characteristics of an airfoil near stall is accomplished most efficiently by solving the Navier-Stokes equations on an arbitrary coordinate system. The numerical generation of boundary-fitted curvilinear coordinate systems[1-7] has greatly increased the range of applicability of finite-difference methods. Partial differential equations can now be solved accurately and efficiently about arbitrary geometric shapes by using such coordinates. General computer algorithms using boundary-fitted curvilinear coordinates can be developed both for grid generation and for solution of partial differential equations.

Generation of optimum boundary-fitted coordinates for the solution of the Navier-Stokes equations at high Reynolds number has been difficult. Previous attempts[3-5] were relatively crude and inefficient compared to the grid-generation techniques used in this research. In the present work, the grid spacing was optimized based upon truncation-

error arguments rather than upon experience. Since boundary-layer theory was used for one of these arguments, the resulting grid systems are referred to as boundary-layer dependent. Boundary-layer-dependent grid systems were generated efficiently for a one-dimensional model equation, for a circular cylinder, and for the NACA 0018 and NACA 6412 airfoils.

An implicit finite-difference method was used to solve partial difference equations on the boundary-layer-dependent grids. Since forward-time explicit solutions of the Navier-Stokes equations result in large computation times due to stability limitations on the time step, backward-time implicit solutions which are unconditionally stable were used to decrease computation time. The solution at each time step in the implicit approach was obtained by using a successive-overrelaxation (SOR) iteration scheme with computation time conserved by not requiring complete convergence at early time steps. If a steady solution existed, additional computational time saving was possible, if the true transient solution was not desired.

First, a one-dimensional model equation was solved to demonstrate the implicit method. Since the model equation has an analytical solution, it enables comparisons of various difference schemes, iterative schemes, and grid systems. Based upon the results of this study with the model equation, a second-order, one-sided, upwind-difference scheme was developed to solve the incompressible Navier-Stokes equations for laminar flow about a cylinder.

The primary objective of this research was to predict the laminar flow and force coefficients for arbitrary airfoils at Reynolds numbers ranging from 4×10^4 to 2×10^5. Solutions in this range hopefully can be compared to experiment without the additional complication of turbulence modeling. Unsteady flow about a NACA 0018 airfoil at zero angle of attack was predicted and compared to available experimental data. Unsteady flow about a NACA 6412 airfoil near stall and at maximum lift was predicted. Solutions about the NACA 6412 airfoil were also compared to experimental observations made in a smoke tunnel.

Curvilinear Grid Systems

The method for generating boundary-fitted curvilinear grid systems requires the numerical solution of a Poisson equation for each coordinate direction.[1-7] The general transformation utilized by the method is depicted for a doubly connected region in Fig. 1. The system of equations for grid generation in the two-dimensional physical (x,y) plane is:

$$\xi_{xx}+\xi_{yy}=P(\xi,\eta) \tag{1a}$$

$$\eta_{xx}+\eta_{yy}=Q(\xi,\eta) \tag{1b}$$

where subscripts denote partial differention. The dependent and independent variables are interchanged by assuming a nonzero Jacobian J so that all finite-difference approximations are accomplished on a rectangular grid system in the transformed (ξ,η) plane, and the system of Eqs. (1) becomes

$$\alpha x_{\xi\xi}-2\beta x_{\xi\eta}+\gamma x_{\eta\eta}=-J^2[x_\xi P(\xi,\eta)+x_\eta Q(\xi,\eta)] \tag{2a}$$

$$\alpha y_{\xi\xi}-2\beta y_{\xi\eta}+\gamma y_{\eta\eta}=-J^2[y_\xi P(\xi,\eta)+y_\eta Q(\xi,\eta)] \tag{2b}$$

where

$$\alpha=x_\eta^2+y_\eta^2$$

$$\gamma=x_\xi^2+y_\xi^2$$

$$\beta=x_\xi x_\eta+y_\xi y_\eta$$

$$J=x_\xi y_\eta-x_\eta y_\xi$$

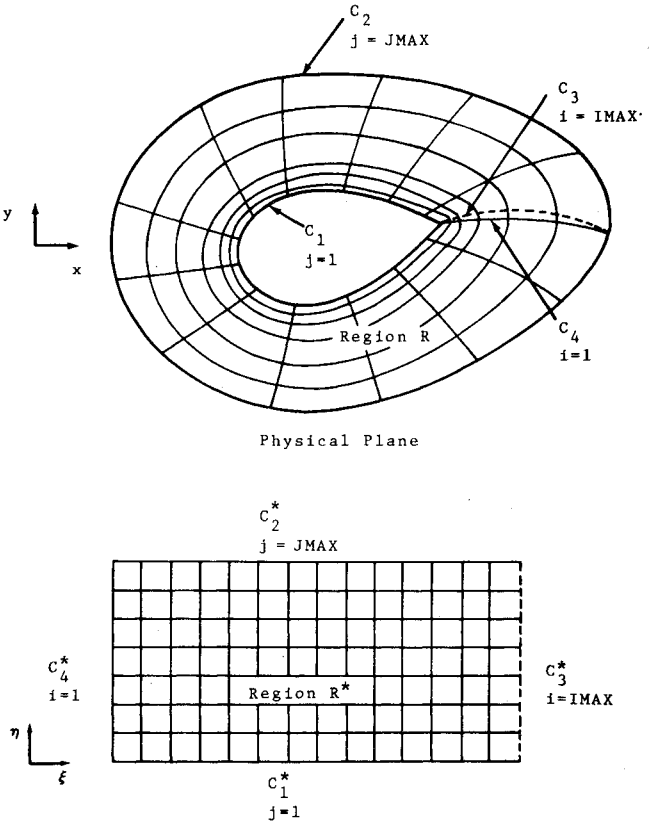

Fig. 1 Doubly connected transformation.

The forcing function used to control the η-line spacing is:

$$Q(\xi,\eta)=-\sum_{k=1}^{K(\xi)}A_k(\xi)\exp[-D(\xi)\,|\eta-\eta_k|] \tag{3}$$

where $A_k(\xi)$, $K(\xi)$, and $D(\xi)$ must be determined and $\eta_k=(k-1)\Delta\eta$.

The coefficient $A_k(\xi)$ controls the η-line spacing. An automated procedure to determine these coefficients was originally developed to require a certain number of points in the boundary layer; however, this procedure was rather inefficient. Another procedure has now been developed which also uses boundary-layer theory to determine the coefficients.

The new automated procedure also aims at minimizing truncation error within the boundary layer and in the remaining regions. Tangential velocity profiles can be calculated by a boundary-layer solution. These profiles could be equated to linear functions of η, thus specifying the η-line spacing within the boundary layer on each ξ line in the physical plane. The derivatives are therefore

$$u_\eta=\text{const.} \tag{4a}$$

$$u_{\eta\eta}=u_{\eta\eta\eta}=u_{\eta\eta\eta\eta}=0,\ \text{etc.} \tag{4b}$$

and, since the procedure is applied on most ξ lines,

$$u_\xi=u_{\xi\xi}=u_{\xi\xi\xi}=u_{\xi\xi\xi\xi}=0,\ \text{etc.} \tag{4c}$$

A truncation-error analysis in the transformed plane for the tangential velocity (variable with maximum normal gradient) in a finite-difference solution would give zero truncation error within the boundary layer, since all higher order derivatives are zero. Equating the linear function to a velocity profile is accomplished by a Newton iteration, and η lines are essentially placed at constant increments in the velocity profiles

such that $u_\eta = \Delta u$ and $u_\xi = 0$ at each point through the boundary layer. Typically, accurate scale factors are obtained with several points in the boundary layer, since the second derivative of the profile with respect to the boundary-layer ordinate does not normally change sign.

Another Taylor series expansion in the variable-grid system in the physical plane[8] appears to contradict the preceding analysis. A diffusive-type truncation error appears in a central-difference representation for

$$u_y = u_\eta|_{CS}/y_\eta|_{CS} - \Delta\eta^2 y_{\eta\eta}|_{CS} u_{yy}/2 + \ldots \tag{5}$$

where $\Delta\eta = 1$ and CS denotes a central-space difference. Thus, there is a truncation error proportional to $y_{\eta\eta}$. Therefore, second derivatives of the grid spacing should be minimized, or at least $y_{\eta\eta}$ should be small compared to y_η. This appears to contradict Eqs. (4), which give zero truncation error for finite $y_{\eta\eta}$; however, even though u_η has no error, u_y has error since $u_y = u_\eta \eta_y$ and η_y has error. Basically, an optimum grid exists such that higher derivatives can be minimized for one variable. Second derivatives of the grid distribution ($y_{\eta\eta}$) may need to be small when other variables are considered and when criteria to optimize the grid spacing are not available. The magnitude of $y_{\eta\eta}$ therefore was minimized outside the boundary layer by preventing large changes in mesh spacing.

A new automated procedure was developed to approximately satisfy the preceding requirements and is based primarily upon on analytical integration of Eq. (1b) with η_{xx} zero with y actually treated as the boundary-layer ordinate. This integration gives

$$(d\eta/dy)^2 = \sum_{k=1}^{K} 2(A_k/D)\{\exp[-D\mu(\eta,\eta_k)] + \mu[\mathrm{sgn}(\eta_k - \eta), 0.0][1.0 - \exp[-D|\eta,\eta_k|]\} \tag{6}$$

where

$$\eta(\eta,\eta_k) = \begin{cases} 0 & \text{if } \eta \le 0 \\ \eta - \eta_k & \text{if } \eta > 0 \end{cases}$$

$$\mathrm{sgn}(\eta_k - \eta) = \begin{cases} +1 & \text{if } \eta_k - \eta \ge 0 \\ -1 & \text{if } \eta_k - \eta < 0 \end{cases}$$

A Blasius profile was utilized for simplicity in the procedure[9,10] for all bodies; thus, the resulting grid systems are referred to as boundary-layer dependent. Optimization of ξ-line spacing could also be accomplished in a similar manner. The optimization could be based on an inviscid pressure distribution with maximum and minimum step-size limits. The forcing function P must then be consistent with the grid spacing to maintain local orthogonality.[9-11]

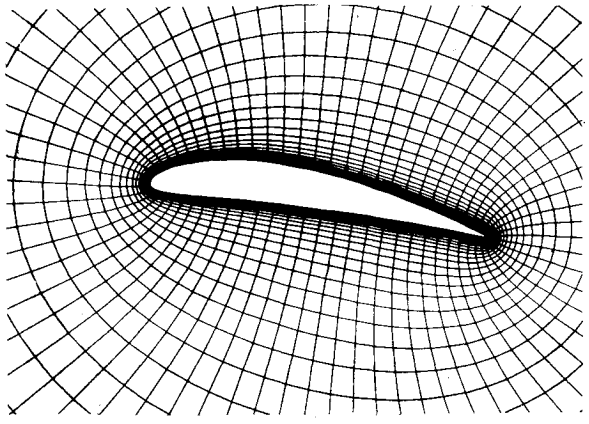

Fig. 2 Boundary-layer dependent grid (NACA 6412, 71×44 grid, $Re = 2\times10^5$).

A sample of a boundary-layer-dependent grid system ($JMAX = 71$, $JMAX = 44$) for a NACA 6412 airfoil at a chord Reynolds number of 2×10^5 is shown in Fig. 2. Grid systems at $Re = 2\times10^6$ were also generated using only 100 s of CDC 6600 computer time for each case. The earlier automated procedure[3] was used to generate the grid systems for the flow about a NACA 0018 airfoil and a NACA 6412 airfoil at a Reynolds number of 4.4×10^4. The new boundary-layer-dependent procedure was used for the solution of a one-dimensional model equation at a Reynolds number of 2×10^6, for a circular cylinder at a Reynolds number of 67, and for a NACA 6412 airfoil at a Reynolds number of 1.67×10^5.

Solution of the One-Dimensional Model Equation

A one-dimensional model equation for the Navier-Stokes equations in Cartesian coordinates is:

$$u_T + uu_y = u_{yy}/Re \tag{7}$$

This transforms to

$$u_T + [u/y_\eta + y_{\eta\eta}/(Re\ y_\eta^3)]u_\eta = u_{\eta\eta}/(Re\ y_\eta^2) \tag{8}$$

with boundary conditions $u = 0$ at $y = 0$, and $u = 1$ at $y = -\infty$. The analytical steady solution of Eq. (7) is:

$$u(y) = -\tanh(Re\ y/2) \tag{9}$$

Equation (7) was solved numerically as an unsteady equation as well as a steady equation with $u_T = 0$, by various difference schemes, by various iterative schemes, and on various mesh systems.[12]

A boundary-layer-dependent mesh was generated for this one-dimensional model equation where $JMAX = 44$, $x = 1$, and $y_\infty = -10$ and used as the standard case. The Reynolds number in the model equation is equal to the square root of 2×10^6 or, approximately, $Re = 1500$, since the viscous-dominant region is inversely proportional to the Reynolds number in the model equation.

A second-order, one-sided, upwind-difference scheme, which is similar but applied differently from other upwind schemes,[13] was used unless otherwise denoted. An example of the upwind difference is:

$$u_\eta = (3u_j - 4u_{j-1} + u_{j-2})/2 + \ldots \text{ if } u_m \ge 0 \tag{10a}$$

$$u_\eta = (-3u_j + 4u_{j+1} - u_{j+2})/2 + \ldots \text{ if } u_m < 0 \tag{10b}$$

where $u_m = [u/y_\eta + y_{\eta\eta}/(Re\, y_\eta^3)]$

Solutions for various Reynolds numbers (200, 1500, 5000, and 2×10^6) were obtained on the same boundary-layer dependent mesh and compared to the theoretical solution and to other methods.[14,15] Comparison of the solutions demonstrated the following:

1) The convergence rate of the implicit solution of the unsteady equation with large time steps was identical to that of the steady equation.

2) The ratio of computer time required by the explicit scheme was 1 for $Re = 2\times10^6$, 60 for $Re = 1500$, and could not even be computed at $Re = 200$.

3) The upwind-difference scheme converged for cell Reynolds numbers ranging from 0.04 to 2×10^6, whereas central-spacing schemes diverged.

4) The upwind scheme produced slightly less maximum error between the numerical and theoretical solution than the central-space scheme at $Re = 1500$ even for a limited number of grid points (6) when the cell Reynolds number was small.

5) The boundary-layer-dependent mesh at $Re = 1500$ produced less maximum error than an exponential mesh or a Cartesian mesh, although the latter had more points in the boundary layer and a step size equal to the smallest step size in

the boundary-layer-dependent mesh. This demonstrated that an optimized variable mesh distribution will minimize truncation error.

Solution of the Navier-Stokes Equations

The time-dependent system of incompressible Navier-Stokes equations expressed in terms of the primitive non-dimensional variables of velocity and pressure which were solved in the transformed (ξ,η) plane are:

$$u_T + u(y_\eta u_\xi - y_\xi u_\eta)/J + v(x_\xi u_\eta - x_\eta u_\xi)/J + uD$$
$$= -y_\eta p_\xi/J + y_\xi p_\eta/J + [(\alpha u_{\xi\xi} - 2\beta u_{\xi\eta} + \gamma u_{\eta\eta})/J^2$$
$$+ (\sigma/J^2)u_\eta + (\tau/J^2)u_\xi]/Re \quad (11a)$$

$$v_T + u(y_\eta v_\xi - y_\xi v_\eta)/J + v(x_\xi v_\eta - x_\eta v_\xi)/J + vD$$
$$= -x_\xi p_\eta/J + x_\eta p_\xi/J + [(\alpha v_{\xi\xi} - 2\beta v_{\xi\eta} + \gamma v_{\eta\eta})/J^2$$
$$+ (\sigma/J^2)v_\eta + (\tau/J^2)v_\xi]/Re \quad (11b)$$

$$D = (y_\eta u_\xi - x_\eta v_\xi - y_\xi u_\eta + x_\xi v_\eta)/J = 0 \quad (11c)$$

$$D_T + [(y_\eta u_\xi - y_\xi u_\eta)^2 + 2(y_\eta v_\xi - y_\xi v_\eta)(-x_\eta u_\xi + x_\xi u_\eta)$$
$$+ (-x_\eta v_\xi + x_\xi v_\eta)^2]/J^2 = -[(\alpha p_{\xi\xi} - 2\beta p_{\xi\eta} + \gamma p_{\eta\eta})/J^2$$
$$+ (\sigma/J^2 P_\eta + (\tau/J^2)p_\xi] \quad (11d)$$

where

$$\sigma = (y_\xi D_1 - x_\xi D_2)/J, \quad \tau = (x_\eta D_2 - y_\eta D_1)/J$$
$$D_1 = \alpha x_{\xi\xi} - 2\beta x_{\xi\eta} + \gamma x_{\eta\eta}, \quad D_2 = \alpha y_{\xi\xi} - 2\beta y_{\xi\eta} + \gamma y_{\eta\eta}$$

The no-slip velocity boundary conditions were imposed on the body surface while uniform freestream conditions were imposed on the upstream half of the circular outer boundary, which had a radius of 10 chord lengths. First-order velocity gradients with respect to η were set to zero and the pressure was set equal to the freestream pressure at the downstream outer boundary, thus permitting the presence of wake. The pressure on the body was calculated by the pressure iteration:

$$p^{(s+1)} = p^{(s)} - \Phi D \quad (12)$$

where (s) denotes the iterate number, not the time level, and Φ is the acceleration parameter.[3]

Second-order-accurate differences were used to approximate spatial derivatives, except for some points adjacent to boundaries. The η derivatives in the velocity divergence D on the body were approximated by second-order-accurate three-point one-sided differences. Second-order-accurate one-sided upwind differences were used to approximate the first derivative terms, with the exception of the pressure-gradient terms in Eqs. (11a and b) and of the velocity divergence D given in Eq. (11c). The upwind difference is given by:

$$u_\xi = (3u_i - 4u_{i-1} + u_{i-2})/2 + \ldots \text{ if } (uy_\eta - vx_\eta) > 0 \quad (13a)$$

or

$$u_\xi = (-3u_i + 4u_{i+1} - u_{i+1})/2 + \ldots \text{ if } (uy_\eta - vx_\eta) < 0 \quad (13b)$$

First-order-accurate two-point upwind differences with the associated artificial viscosity were necessary at some points adjacent to boundaries, but did not pose a serious problem since the artifical viscosity could be minimized by a very fine grid-spacing adjacent to the body. All second derivatives, the pressure gradient terms, and the velocity divergence were approximated by central differences.

Since a first-order-accurate two-point backward-time difference was used to approximate time derivatives, a system of linearized simultaneous difference equations was obtained for each time step. Therefore, the method of solution was implicit. SOR iteration was used to solve the system of equations at each time step. The SOR iteration was simple to program, and perhaps caused fewer difficulties due to nonlinearities and coupling. Efficiency was gained by not requiring convergence during early time steps after an inviscid initial guess.[1] Thus, a truly time-dependent solution was neither obtained nor desired at early time steps.

Discussion of Results

Circular Cylinder

The flow about a circular cylinder was investigated to evaluate the effect of time step on the solution. The steady flow about a circular cylinder at a Reynolds number of 20 (based on diameter) and the unsteady flow with shedding separation bubbles at a Reynolds number of 67 were investigated. Mesh systems with $JMAX = 37$ and $JMAX = 60$ were used.

A steady value of 2.0534 for the drag coefficient, compared to experimental values[16,17] of 2.0-2.2, was obtained numerically, with time steps of both 0.04 and 0.08 for the circular cylinder at a Reynolds number of 20. Solutions were continued to a time of 64.3, or the equivalent of moving the body distance of 64.3 diameters, with no change over the last 30 diameters. An asymmetry in the pressure distribution on the upper and lower surfaces caused a small steady lift coefficient of -0.01. Time steps up to 0.5 could be used at later time steps. For this case, a steady solution could be obtained efficiently with 10 min of CDC 6600 computer time.

Unsteady solutions for a circular cylinder at a Reynolds number of 67 were obtained using various combinations of time steps. After starting with a time step of 0.001 for 10 steps, time steps of 0.01 and 0.04 were used. The drag coefficient for the 0.01 case was increasing beyond the experimental value of approximately 1.31,[16] and was discontinued because of the computer time requirements at this small time step. The 0.04 case had a lag in time, characteristic of large time steps for a first-order, time-implicit method, but approached the level of 1.30 with an oscillation of ± 0.003 amplitude and a period of 7 time units.

The numerical solution with a time step of 0.01 for the circular cylinder at a Reynolds number of 67 was continued from a time of 64.3 with time steps of 0.04, 0.08, and 0.16. For the 0.04 time step, the drag coefficient time history showed an abrupt increase in C_D whic finally leveled at 1.31. For the 0.08 time step, the drag coefficient time history was nearly the same as the 0.04 restart, until a time of about 90 units, when the drag coefficient dropped abruptly. For the 0.16 time step, the drag coefficient time history was nearly the same up to a time of 135. The pattern of the two shedding separation bubbles behind the cylinder became more symmetric and diffused for the large time steps. More than two bubbles could not be identified, regardless of the time step, because of insufficient grid resolution downstream. The experimental[18] pressure drag coefficient for a cylinder with splitter plate (which enforces base symmetry) is 0.80, whereas an experimental pressure value of 0.9 occurs for no splitter plate.[19] This demonstrates a possible decrease in a steady drag coefficient of 0.1. The pressure-drag coefficient for the 0.04 restart was 0.92. The drag coefficient decreases by 0.1 for the 0.16 time step. Therefore, solutions at larger time steps appear to be tending toward a steady solution (comparable to the case with a splitter plate) due to incorrect resolution of the unsteady phenomena.

NACA 0018

Since difficulty had been encountered previously in the numerical solution for the laminar flow about a NACA 0018

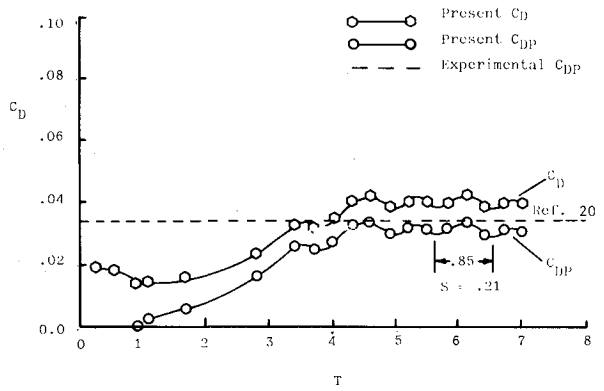

Fig. 3 Predicted drag coefficient time history (NACA 0018, $Re = 41,400$, $\phi = 0$ deg).

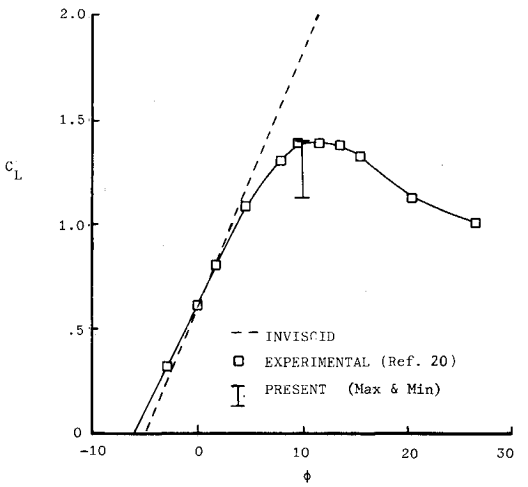

Fig. 4 Lift coefficient curve (NACA 6412, $Re = 167,000$).

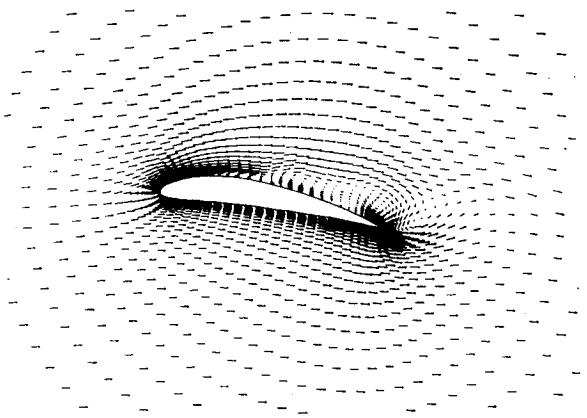

Fig. 5 Predicted velocity vectors (NACA 6412, $Re = 41,400$, $\phi = 10$ deg, $T = 5.5$).

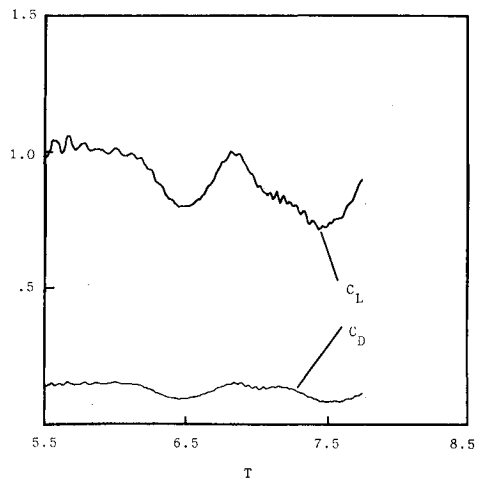

Fig. 6 Predicted lift and drag time histories (NACA 6412, $Re = 41,400$, $\phi = 10$ deg).

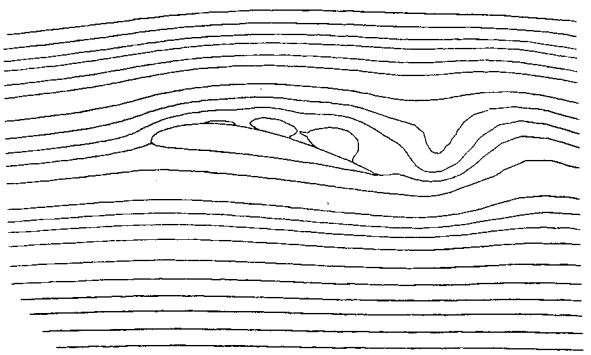

Fig. 7 Predicted streamline contours (NACA 6412, $Re = 41,400$, $\phi = 10$ deg, $T = 5.5$).

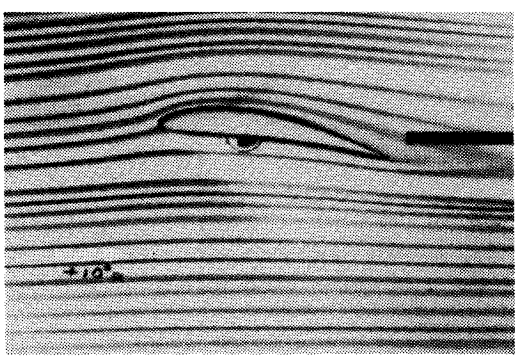

Fig. 8 Experimental flow visualization (NACA 6412, $Re = 46,000$, $\phi = 10$ deg).

airfoil (with a sharp trailing edge, a chord Reynolds number of 4.14×10^4, and zero angle of attack),[3] second-order, one-sided upwind differences for first derivatives, instead of central-space differences, were used in the present work. The implicit method was successful for a time step of 0.001 and a maximum of two iterations per time step.[4] Approximately 2 h of CDC 6600 computer time was required to obtain a converged solution.

The NACA 0018 solution is unsteady and has an asymmetry in the pressure distribution as for the cylinder. The lift coefficient ($C_L = -0.033$ at $T = 7$) oscillated slightly with the shedding of bubbles and would not be expected to be exactly zero. The Strouhal number based on airfoil thickness agrees with the experimental Strouhal number of 0.21 for a cylinder, as shown in Fig. 3. The average value of the drag coefficient is a horizontal asymptote, and pressure drag of 0.032 compares to an experimental pressure drag[20] of 0.034.

NACA 6412

Numerical solutions for the laminar flow about a NACA 6412 cambered airfoil with a rounded trailing edge were obtained at a Reynolds number of 4.14×10^4 for angles of attack of -4.7, 0, 10, and 16 deg. The solution about a NACA 6412 airfoil at a Reynolds number of 1.67×10^5 for a 10-deg angle of attack[5] also was obtained. The solutions were again obtained for 10-deg angle of attack to produce a movie of the bubbles shedding.[21] For these Reynolds numbers, the

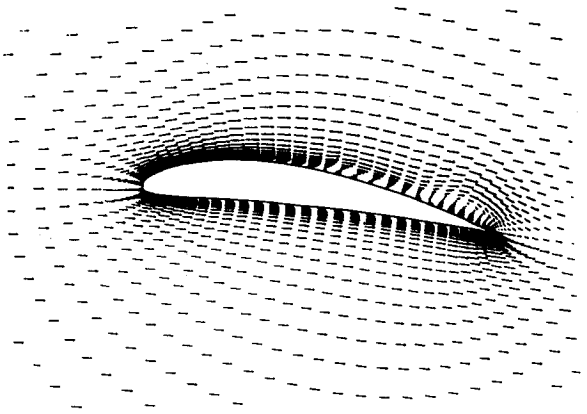

Fig. 9 Predicted velocity vectors (NACA 6412, $Re = 167{,}000$, $\phi = 10$ deg, $T = 4.83$).

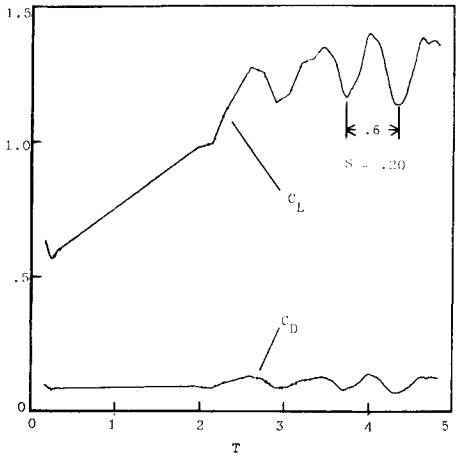

Fig. 10 Predicted lift and drag time histories (NACA 6412, $Re = 167{,}000$, $\phi = 10$ deg).

airfoil at 10-deg angle of attack is near stall and, essentially, at maximum lift, as seen in Fig. 4.

The numerical solution for the NACA 6412 at Reynolds number of 4.14×10^4 was very unsteady, because of the shedding of large separation bubbles. A velocity vector plot is shown in Fig. 5. A lift and drag time history of the restarted solution is given in Fig. 6. Streamline contours are given in Fig. 7 for comparison with the experimental smoke path lines shown in Fig. 8. Although the unsteady flowfield and the separation point of the numerical solution qualitatively matched the experimental field quite well, small discrepancies can be identified.

The numerical solution for the flow about a NACA 6412 airfoil at Reynolds number of 1.67×10^5 was also unsteady, but the bubbles were smaller. A velocity vector plot is shown in Fig. 9, and lift and drag time histories of the solution are given in Fig. 10. The dominant frequency agrees with the Strouhal number for a cylinder, and the maximum lift agrees with the average experimental lift coefficient.[20] The drag does not agree, possibly due to numerical error in the drag integration and poor resolution on the top surface. Streamline contours are given in Fig. 11 for comparison with the experimental smoke path shown in Fig. 12. Again, although the separation point matched the experimental field quite well, small discrepancies can also be identified.

The discrepancies between the numerically predicted streamline contours and the experimental smoke paths are mainly on the top surface of the airfoil. The separated bubbles in the smoke tunnel are thinner than the predicted bubbles, and the smoke lines in the inviscid region above the

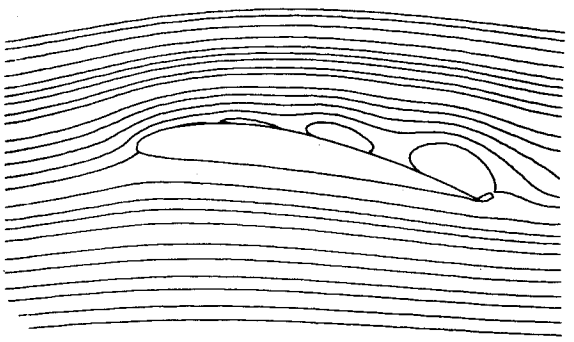

Fig. 11 Predicted streamline contours (NACA 6412, $Re = 167{,}000$, $\phi = 10$ deg, $T = 4.83$).

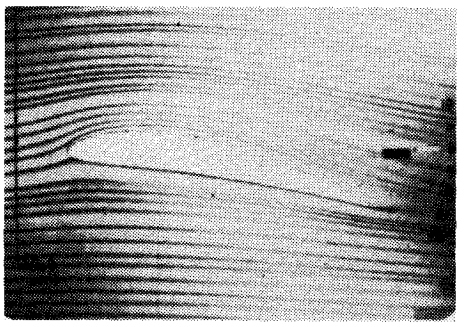

Fig. 12 Experimental flow visualization (NACA 6412, $Re = 167{,}000$, $\phi = 10$ deg).

nose are closer to the airfoil. The airfoil chord for the Reynolds number of 167,000 was 14 in. and the wall was only 1½ chords away. Streamlines above the nose, calculated by an inviscid solution with the wall at 10 chords, compared well with the viscous solution. With the wall at 1½ chords, calculated streamlines above the nose compared well with the smoke paths. This implies that wall effect could cause the discrepancy. The size of the bubbles would be affected in a similar manner.

Two other possible reasons for these discrepancies are of concern. First, the unsteadiness of the flow was not captured in the photograph, and can only be identified by the smearing of the smoke. Second, turbulence is possible in the smoke tunnel, but not in the laminar numerical solution. Leading-edge stall is a laminar phenomenon, and the stalled flow pattern given by Prandtl[22,23] is similar to the separated flow pattern shown in Fig. 11. However, after the flow separates, turbulence may affect the bubbles even at these Reynolds numbers. More precise experimental measurements are planned in the future to resolve these issues.

V. Conclusions

The Navier-Stokes equations were solved for an airfoil at angle of attack, with a boundary-layer-dependent mesh system, by an implicit method. The mesh systems were generated automatically for any Reynolds number in only 100 s of CDC 6600 computer time. Optimization of the mesh systems was based upon boundary-layer profiles for laminar flow over a flat plate. Justification of the mesh distribution and the present second-order, one-sided, upwind-difference scheme was provided by comparisons of numerical solutions with the analytical solutions of a one-dimensional model equation. The upwind scheme was used in the solution of both steady and unsteady flows about a circular cylinder. It was determined that large time steps could be used for steady flow, resulting in as low as 10 min of computer time. Small time steps were required to accurately describe the unsteady flows, normally resulting in about 2 hr of computer time.

Unsteady laminar flows about NACA airfoils near stall displayed unsteady shedding of separation bubbles. Experimental flow visualizations for the NACA 6412 airfoil confirmed the predicted solutions qualitatively. An exhaustive experimental study for the unsteady laminar flow is needed to quantitatively compare the solutions without the additional problem of modeling turbulence.

Acknowledgment

The authors are thankful to W. Hankey, J. Shang, and U. Ghia for their many useful suggestions, and to W. Cooper for assistance in preparing the contour plots.

References

[1] Thompson, J. H., Thames, F. C., and Mastin, C. W., "Automated Numerical Generation of Body-Fitted Curvilinear Coordinate System for Field Containing Any Number of Arbitrary Two-Dimensional Bodies," *Journal of Computational Physics*, Vol. 15, July 1974, pp. 299-319.

[2] Thames, F. C., "Numerical Solution of the Incompressible Navier-Stokes Equations about Arbitrary Two-Dimensional Bodies," Ph.D. Thesis, Dept. of Aerophysics and Aerospace Engineering, Mississippi State Univ., May 1975.

[3] Hodge, J. K., "Numerical Solution of Incompressible Laminar Flow about Arbitrary Bodies in Body-Fitted Curvilinear Coordinates," Ph.D. Thesis, Dept. of Aerophysics and Aerospace Engineering, Mississippi State Univ., Dec. 1975.

[4] Thompson, J. F., Thames, F. C., Hodge, J. K., Shanks, S. P., Reddy, R. N., and Mastin, C. W., "Solutions of the Navier-Stokes Equations in Various Flow Regimes on Fields Containing any Number of Arbitrary Bodies Using Body-Fitted Coordinate Systems," 5th International Conference on Numerical Methods in Fluid Dynamics, Euschede, The Netherlands, 1976.

[5] Stone, A. L., "A Numerical Solution of the Navier-Stokes Equations for Flow over an Arbitrary Airfoil," M.S. Thesis (GAE/AE/76D-5), Air Force Institute of Technology, Wright-Patterson AFB, Ohio, Dec. 1976.

[6] Thompson, J. F., Thames, F. C., and Mastin, C. W., "Boundary-Fitted Curvilinear Coordinate Systems for Solution of Partial Differential Equations on Fields Containing Any Number of Arbitrary Two-Dimensional Bodies," NASA CR-2729, 1977.

[7] Thompson, J. F., Thames, F. C., and Mastin, C. W., "TOMCAT—A Code for Numerical Generation of Boundary-Fitted Curvilinear Coordinate Systems on Fields Containing Any Number of Arbitrary Two-Dimensional Bodies," *Journal of Computational Physics*, Vol. 24, July 1977, pp. 274-302.

[8] Warsi, Z.U.A. and Thompson, J. F., "Machine Solutions of Partial Differential Equations in the Numerically Generated Coordinate Systems," Rept. MSSU-EIRS-ASE-77-1, Engineering and Industrial Research Station, Mississippi State Univ., 1976.

[9] Ghia, U., Hodge, J. K., and Hankey, W. L., "Surface-Oriented Coordinates for Arbitrary Bodies in High Re-Flow: An Optimization Study," Open Forum Presentation at AIAA 3rd Computational Fluid Dynamics Conference, June 1977.

[10] Ghia, U., Hodge, J. K., and Hankey, W. L., "An Optimization Study for Generating Surface-Oriented Coordinates for Arbitrary Bodies in High Reynolds Number Flows," AFFDL-TR-77-117, Dec. 1977.

[11] Plant, T. J., "An Exact Velocity Potential Solution of Steady Compressible Flow over Arbitrary Two-Dimensional and Axisymmetric Bodies in Simply Connected Fields," AFFDL-TR-77-116, Dec. 1977.

[12] Hodge, J. K. and Hankey, W. L., "Implicit Methods for Model Equation," AFFDL Tech. Memo. (to be published), 1979.

[13] Atias, M., Wolfshtein, M., and Israeli, M., "A Study of the Efficiency of Various Navier-Stokes Solvers," *Proceedings of the AIAA 2nd Computational Fluid Dynamics Conference*, Hartford, Conn., June 1975, pp. 81-90.

[14] MacCormack, R. W. and Baldwin, B. S., "A Numerical Method for Solving the Navier-Stokes Equations with Application to Shock-Boundary Layer Interactions," AIAA Paper 75-1, Pasadena, Calif., 1975.

[15] Roscoe, D. F., "New Methods for the Derivation of Stable Difference Representations for Differential Equations," *Journal of the Institute of Mathematical Applications*, Vol. 16, 1975, pp. 291-301.

[16] Tritton, D. J., "Experiments on the Flow Past a Circular Cylinder at Low Reynolds Numbers," *Journal of Fluid Mechanics*, Vol. 6, 1937, p. 547.

[17] Nishioka, M. and Sato, H., "Measurements of Velocity Distributions in the Wake of a Circular Cylinder at Low Reynolds Numbers," *Journal of Fluid Mechanics*, Vol. 65, Pt. 1, Aug. 1974, pp. 97-112.

[18] Grove, A. A., Shair, F. H., Peterson, E. E., and Acrivos, A., "An Experimental Investigation of the Steady Separated Flow Past a Circular Cylinder," *Journal of Fluid Mechanics*, Vol. 19, Pt. 1, May 1964, pp. 60-80.

[19] Thom, A., "The Flow Past Circular Cylinders at Low Speeds," *Proceedings of the Royal Society of London*, A141, 1933, p. 651.

[20] Jacobs, E. N. and Sherman, A., "Airfoil Characteristics as Affected by Variations of the Reynolds Number," NACA Rept. 596, 1937.

[21] Hodge, J. K. and Cooper, W. H., "Solution of Navier-Stokes Equations for Airfoils at Angle of Attack Near Stall," AFFDL-TM-77-94-FXM, Nov. 1977.

[22] Schlichting, H., *Boundary Layer Theory*, 6th Ed., McGraw-Hill Book Co., New York, 1968, p. 36.

[23] Batchelor, G. K., *An Introduction to Fluid Dynamics*, Cambridge University Press, Cambrige, 1967, p. 352, plate 7.